Role of Solution Structure in Solid Electrolyte Interphase Formation on Graphite with LiPF6 in Propylene Carbonate

ARTICLE *in* THE JOURNAL OF PHYSICAL CHEMISTRY C · NOVEMBER 2013

Impact Factor: 4.77 · DOI: 10.1021/jp409765w

6 AUTHORS, INCLUDING:

Mengyun Nie
Dalhousie University
24 PUBLICATIONS **201** CITATIONS
SEE PROFILE

Daniel P. Abraham
Argonne National Laboratory
148 PUBLICATIONS **3,261** CITATIONS
SEE PROFILE

Yanjing Chen
29 PUBLICATIONS **393** CITATIONS
SEE PROFILE

THE JOURNAL OF PHYSICAL CHEMISTRY C

Article

pubs.acs.org/JPCC

Role of Solution Structure in Solid Electrolyte Interphase Formation on Graphite with $LiPF_6$ in Propylene Carbonate

Mengyun Nie,[†] Daniel P. Abraham,[‡] Daniel M. Seo,[†] Yanjing Chen,[†] Arijit Bose,[†] and Brett L. Lucht*[,†]

[†]University of Rhode Island, Kingston, Rhode Island 02881, United States

[‡]Argonne National Laboratory, Argonne, Illinois 60438, United States

Supporting Information

ABSTRACT: An investigation of the interrelationship of cycling performance, solution structure, and electrode surface film structure has been conducted for electrolytes composed of different concentrations of $LiPF_6$ in propylene carbonate (PC) with a binder-free (BF) graphite electrode. Varying the concentration of $LiPF_6$ changes the solution structure, altering the predominant mechanism of electrolyte reduction at the electrode interface. The change in mechanism results in a change in the structure of the solid electrolyte interface (SEI) and the reversible cycling of the cell. At low concentrations of $LiPF_6$ in PC (1.2 M), electrochemical cycling and cyclic voltammetry (CV) of BF graphite electrodes reveal continuous electrolyte reduction and no lithiation/delithiation of the graphite. The solution structure is dominated by solvent-separated ion pairs ($Li^+(PC)_4//PF_6^-$), and the primary reduction product of the electrolyte is lithium propylene dicarbonate (LPDC). At high concentrations of $LiPF_6$ in PC (3.0−3.5 M), electrochemical cycling and CV reveal reversible lithiation/delithiation of the graphite electrode. The solution structure is dominated by contact ion pairs ($Li^+(PC)_3PF_6^-$), and the primary reduction product of the electrolyte is LiF.

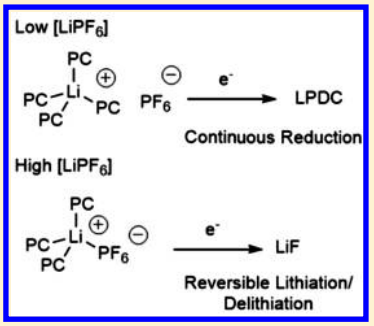

INTRODUCTION

Since the initial commercialization of lithium ion batteries (LIBs) in 1991, the LIB market has rapidly grown to dominate the portable electronic market and is currently expanding into the electric vehicle market. During this time, there have been significant advances in the development of both anode and cathode materials for LIBs.[1] However, advances in the development of electrolytes for LIB have progressed more slowly.[2] One of the most important components of the LIB is the solid electrolyte interphase (SEI) generated on the surface of the graphitic anode during the first few charging cycles via the reductive decomposition of the electrolyte.[3−10] Ideally, the SEI functions as a passivation layer and is lithium ion conducting but electrically insulating, allowing lithium ions to intercalate and deintercalate the electrode while preventing electrolyte reduction at the anode surface. While there has been significant research on the structure and properties of the anode SEI,[3−10] there have been few investigations on the role of electrolyte solution structure in the SEI formation mechanism.[11,12]

There has recently been increased interest in developing a better understanding of the solution structure of electrolytes for lithium ion batteries. The lithium cation coordination sphere has been investigated by IR, NMR, Raman, DSC, MS, and computational methods.[13−20] In electrolyte solutions with weakly coordinating anions and polar aprotic solvents, including propylene carbonate (PC), ethylene carbonate (EC), and acetonitrile, the coordination sphere of the Li cation typically contains four solvent molecules, but ion pairing is also frequently observed.[20] The solvated cations have an important role in the reaction mechanism and properties of the SEI. Understanding how solvation influences the solution structure and reactivity of lithium complexes with weakly coordinating anions at the anode interface is very difficult due to rapid solvent exchange on the lithium cation, the presence of different solvent molecules within common electrolytes resulting in mixed solvation, the possibility of ion pairing, and the inhomogeneous nature of the surface reactions. Developing a better understanding of the role of electrolyte solution structure on SEI formation is critical for the development of superior LIBs.

The difference in cycling performance between EC- and PC-based electrolytes with graphite anodes has long been a mystery in the field of lithium batteries.[21] Electrolytes containing EC have good cycling performance, which is typically attributed to the formation of a stable anode SEI.[5,6] Alternatively, electrolytes containing PC have poor cycling performance due to continuous electrolyte reduction due to the lack of the formation of a stable anode SEI.[22] There have been numerous investigations into the differences in cycling behavior. Most of these investigations attribute the differences to the cointercalation of PC solvent molecules with the Li cation into the graphite sheets, which leads to exfoliation of the graphite.[23−26] Other investigations attribute the differences to the physical properties of the electrolyte reduction products.[27−29] In some cases, good cycling performance has been observed when PC-

Received: October 1, 2013
Revised: November 7, 2013
Published: November 13, 2013

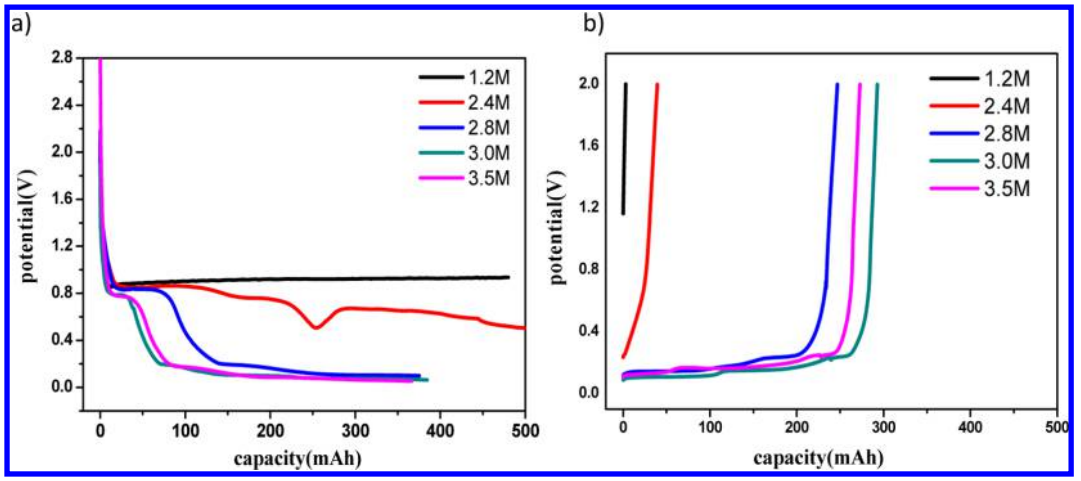

Figure 1. Potential versus capacity curves for BF-graphite/Li cells cycled with five concentrations of $LiPF_6$/PC electrolytes: (a) lithium intercalation profiles, and (b) lithium deintercalation profiles.

based electrolytes contain SEI forming additives.[30−32] In these cases, the additives are preferentially reduced on the anode surface to generate a stable SEI preventing continuous PC reduction. In other investigations, reversible cycling of PC electrolytes has been observed at high concentrations of $LiPF_6$.[12,33]

We have recently reported the use of binder-free (BF) graphite electrodes with integrated TEM grids for characterization of the anode SEI.[34−36] In this Article, we report an investigation of the electrochemical properties, solution structure, anode SEI structure, and SEI formation mechanism for electrolytes containing various concentrations of $LiPF_6$ in PC with a BF graphite electrode. The electrochemical properties have been investigated via a combination of cyclic voltammetry and galvanostatic cycling. The solution structure has been investigated via a combination of IR spectroscopy and DOSY nuclear magnetic resonance (NMR) spectroscopy. The anode SEI has been characterized via a combination of transmission electron microscopy (TEM) with energy dispersive X-ray spectroscopy (EDX), NMR spectroscopy of D_2O extracts from cycled anodes, and XPS. This combination of techniques has provided significant new insights into the role of solution structure in SEI formation mechanisms.

EXPERIMENTAL SECTION

Preparation of Binder-Free Electrodes. Binder-free electrodes are made by electrophoretic deposition (EPD). In this method, graphite particles (SFG-6, TIMCAL, 5 g/L) are suspended in acetonitrile solution by ultrasonication followed by the addition of triethylamine (1 mL/L).[34] A copper current collector is immersed in the EPD bath, and a DC potential of 50 V is applied for 2 min. Graphite particles are deposited evenly on the copper surface to yield a binder-free (BF) graphite electrode. The electrode is placed in a vacuum oven at ∼120 °C overnight to dry the electrode, and then transferred to an argon-filled glove box.

Preparation of Electrolyte Coin Cells. Propylene carbonate was used to dissolve various concentrations of $LiPF_6$. Five PC/$LiPF_6$ electrolytes with different concentrations were prepared: 1.2, 2.4, 2.8, 3.0, and 3.5 M $LiPF_6$/PC. Binder-free graphite electrodes were prepared with copper TEM grids integrated into the binder-free graphite electrode.[36] Cell assembly was conducted in an Ar-atmosphere glovebox (<1 ppm H_2O). Cells experience one galvanostatic charge/discharge cycle at a $C/20$ rate from 2.0 to 0.05 V by an Arbin BT2000 battery cycler at 25 °C.

Cyclic Voltammetry. Cyclic voltammetry was conducted in two-electrode (BF-graphite/Li) CR2032 coin cells with a Princeton Versa STAT 3 at 20 °C. The scan rate was 0.05 mV/s from 0.05 to 2 V. Three scans were conducted for each cell.

IR and DOSY NMR Spectroscopy. Diffusion-ordered nuclear magnetic resonance spectroscopy (DOSY NMR) and infrared (IR) spectroscopy were conducted on pure electrolyte samples.

The Simulated Echo pulse sequence (STEBPGP1S) is used for DOSY experiments. According to the Stejskal−Tanner equation (eq 1), upon adjusting the gradient strength (G_i) from 2% to 95%, the attenuated signal strengths of peaks (I) on ^{7}Li and ^{19}F are detected.

$$I = I_0 \exp\left[- D(2\pi\gamma G i\delta)^2\left(\Delta - \frac{\delta}{3}\right)\right] \quad (1)$$

where I is the intensity of the monitored peak, and γ is the gyromagnetic ratio of the nucleus under investigation. The length of the gradient pulse (δ) and diffusion time (Δ) have been optimized for the DOSY measurements. The data have been analyzed by Bruker Topspin software, and 32 single spectra with varying gradients strength have been taken to provide 32 points in experimental data plot. Linear fitting of a plot of $\ln(I)$ versus G_i^2 provides the diffusion coefficient of monitored nuclei.

FTIR was measured by a Bruker TENSOR 27 spectrometer with an ATR accessory. FTIR bands were deconvoluted with the combination of Gaussian/Lorentzian function. The area of deconvoluted bands was collected, and the relative areas of uncoordinated solvent and coordinated solvent were calculated. The concentrations of coordinated and uncoordinated solvent were calculated with the assumption that IR bands of uncoordinated and coordinated solvent have equal sensitivity.

TEM Imaging and EDX. Cycled cells were disassembled in an Ar-atmosphere glovebox (<1 ppm H_2O). TEM grids were extracted from cycled coin cells and rinsed with anhydrous dimethyl carbonate (DMC, Acros) and then dried overnight. Imaging was conducted using a JEOL JEM-2100F TEM (Peabody, MA) at 160 kV. Energy-dispersive X-ray spectroscopy or EDX (model INCAx-act, Oxford Instrument, UK) was

dx.doi.org/10.1021/jp409765w | J. Phys. Chem. C 2013, 117, 25381−25389

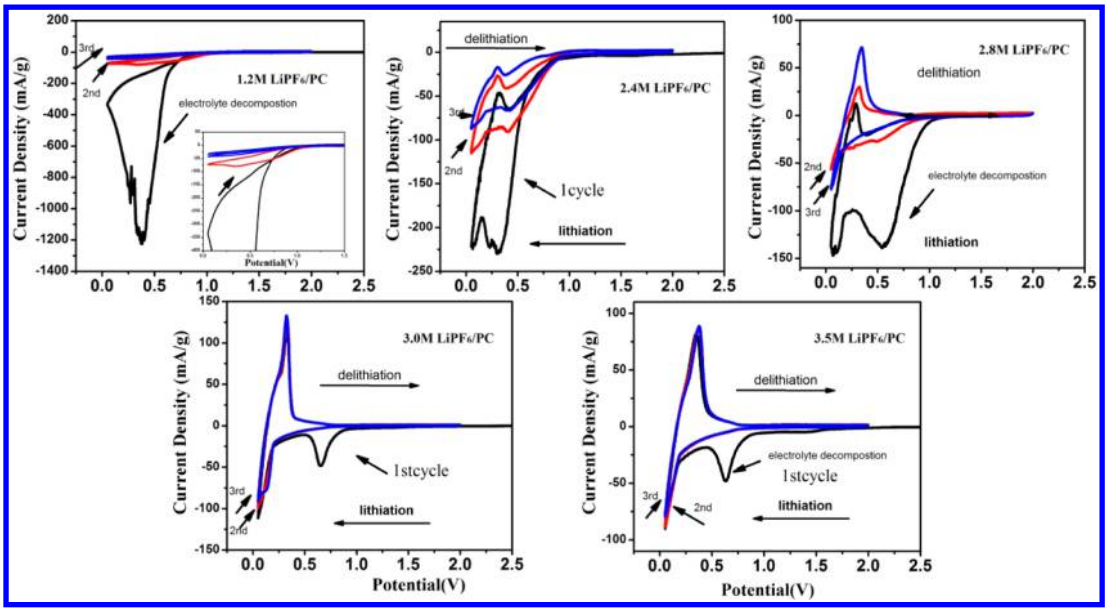

Figure 2. Cyclic voltammograms of BF-graphite/Li system in five concentrations of $LiPF_6$/PC electrolytes cycled between 2 and 0.05 V with 0.05 mV/s.

used to detect elements on the surface of graphite anode. To detect the element composition at different areas, multiple locations from the edge to the center were probed by EDX during imaging. The diameter of EDX beam was 10 nm. Low-dose imaging was employed to minimize the electron beam-induced changes to the organic components of SEI layers.

XPS Analysis of Electrodes. XPS was conducted on BF-graphite electrodes before and after cycling. After being cycled, the electrodes were rinsed with DMC and dried overnight in vacuum. The X-ray photoelectron spectroscopy (XPS) was obtained on a PHI 5500 system using Al, Kα radiation ($h\nu$ = 1486.6 eV) under ultrahigh vacuum conditions; the XPS data were collected at multiple locations of cycled graphite electrodes. The C 1s, O 1s, F 1s, P 2p spectra were calibrated on the basis of the C1s graphite peak binding energy at 284.5 eV.

NMR Analysis of Electrodes. Multinuclear and multi-dimensional NMR analyses were conducted on a Bruker Avance III 300 MHz NMR spectrometer. Electrodes were rinsed with DMC to remove residual electrolyte and dried in a vacuum. The graphite electrodes were then extracted in an Ar glovebox with high-purity D_2O freshly opened from a sealed ampule and analyzed by ^1H, ^{13}C, DEPT-135, HSQC, and COSY NMR spectroscopy.

RESULTS AND DISCUSSION

Electrochemical Cycling Performance. The BF graphite/Li coin cells have been cycled with $LiPF_6$/PC electrolyte with five different concentrations of $LiPF_6$. As shown in Figure 1, the potential profile of the coin cell cycled in 1.2 M $LiPF_6$/PC electrolyte is typical of graphite with PC-based electrolytes as reported previously.[12,29] A long plateau is observed at 0.9 V vs Li, consistent with continuous electrolyte reduction and an absence of lithium intercalation into graphite resulting in very poor columbic efficiency (CE, ~4%). When the concentration is increased to 2.4 M, the cell potential gradually drops from 0.9 to ~0.4 V, but very little reversible capacity (CE ≈ 10%) is obtained. Significant changes are observed when the concentration of $LiPF_6$ is increased to 2.8 M. The cells cycle with much higher efficiency (66%), the shoulder characteristic of electrolyte reduction at ~0.9 V is significantly reduced, and lithium ion intercalation is observed at 0.2−0.05 V. The plateau at ~0.9 V is further suppressed in cells cycled with 3.0 and 3.5 M electrolytes. The delithiation capacities were 297 and 273 mAh, while the CE was approximately 80% for both concentrations of $LiPF_6$.

Cyclic Voltammetry. Cyclic voltammetry is a complementary electrochemical method to constant current cycling, which provides more detail about the reactions of the electrolyte with the electrode surface. The first three consecutive cyclic voltammograms of $LiPF_6$/PC electrolytes with different concentrations of $LiPF_6$ are provided in Figure 2. The initial cathodic processes are critical to the operation of lithium ion batteries due to the reduction reactions of the electrolyte (2.0−0.3 V vs Li), which result in the formation of the solid electrolyte interface (SEI) during the initial lithiation cycles. The SEI formation is then followed by lithium ion intercalation into the graphite (0.3−0.05 V vs Li). The anodic processes from 0.05 to 2 V are typically characterized by deintercalation of Li^+ from graphite.

The first cathodic sweep of the BF-graphite electrode with 1.2 M $LiPF_6$/PC contains a strong peak at 0.36 V vs Li (I_{pc} = −4.4 mA), suggesting a significant reductive decomposition of the electrolyte. The onset of the electrolyte reduction begins at ~0.9 V, which is consistent with the plateau observed in constant current cycling, as discussed above. This cathodic peak is consistent with the reductive decomposition of PC.[12,29] The anodic sweep contains no observable peaks, suggesting that the electrolyte reduction is irreversible and that there is no lithium ion deintercalation from the graphite. The second cathodic scan is similar, although the intensity of the electrolyte reduction peak at 0.33 V has lower current. When the concentration of $LiPF_6$ is increased to 2.4 M, two cathodic peaks are observed, E_{pc} = 0.32 V and E_{pc} = 0.1 V, respectively. The first peak is attributed to the reductive decomposition of electrolyte and only exists in the first cycle, while the second peak is attributed to lithium intercalation. Subsequent CV scans contain the

dx.doi.org/10.1021/jp409765w | J. Phys. Chem. C 2013, 117, 25381−25389

typical reversible peaks, starting from ~0.25 V, characteristic of Li^+ insertion and deinsertion from graphite.

When the concentration of $LiPF_6$ is further increased to 2.8 M, two peaks are still observed during the first cathodic process. However, the current of initial reduction peak is reduced and the peak occurs at higher potential, E_{pc} = 0.56 V. In addition, the intensity of peaks from lithiation is increased. The anodic scan reveals greater intensity for the peak associated with delithiation, and subsequent scans reveal reversible intercalation/deintercalation of lithium. At very high concentrations of $LiPF_6$ (3.0 and 3.5 M), the initial reduction peak on the first cathodic scan has much weaker intensity (0.12 mA) and is further shifted to higher potential (0.65 V). The shift of the irreversible reduction peak to higher potential at higher concentration of $LiPF_6$ also coincides with an onset of reversible lithium ion intercalation/deintercalation and reversible cycling of lithium ion cells.

IR Spectra of $LiPF_6$/PC Electrolytes. Infrared (IR) spectra were obtained of $LiPF_6$/PC solutions at various concentrations of $LiPF_6$. The IR spectrum of pure PC contains a strong C═O stretching vibration at 1789 cm^{-1} and a weaker band at 1800 cm^{-1}. Addition of 1.2 M $LiPF_6$ to PC results in changes in the IR spectra. The C═O absorptions at 1789 and 1800 cm^{-1} decrease in intensity, and new peaks at 1770 and 1752 cm^{-1} characteristic of C═O absorptions for PC coordinated to Li^+ are observed (Figure 3). In addition, a new absorption characteristic of $LiPF_6$ is observed at 844 cm^{-1}. Further increases in the concentration of $LiPF_6$ result in additional changes to the IR spectra. Upon increasing the concentration of $LiPF_6$ to 2.8 M, the C═O absorptions of uncoordinated PC (1789 and 1800 cm^{-1}) decrease and are replaced by the absorptions at 1770 and 1752 cm^{-1}. Similar changes are observed for the C−O absorption bands. The peak associated with uncoordinated PC (1180 cm^{-1}) is gradually replaced by coordinated PC (1210 cm^{-1}) with increasing concentration of $LiPF_6$ (Supporting Information Figure SI1), and the absorption for $LiPF_6$ is also changed. While the peak at 844 cm^{-1} is still present, two new absorptions at 877 and 834 cm^{-1} are observed (Figure 3).

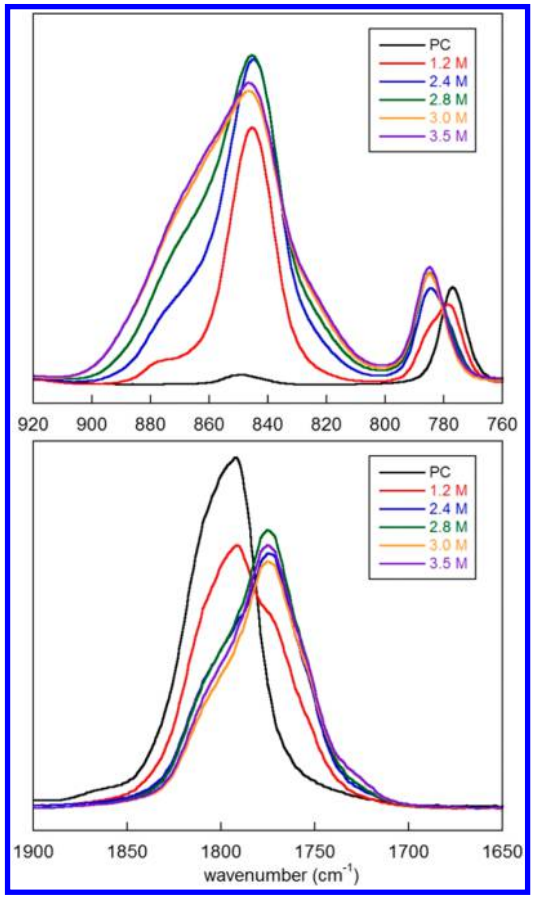

Figure 3. FTIR spectra of five concentrations of $LiPF_6$/PC electrolytes at selected ranges.

The relative area of the IR bands of the C═O absorptions for coordinated and uncoordinated PC has been modeled (Supporting Information Figures SI2 and SI3). The relative areas of coordinated and uncoordinated PC are used to estimate the number of PC molecules coordinated to the Li cation using eq 2, where $C_{PC\,C}$, $C_{PC\,UC}$, and C_{Li} are the concentrations of coordinated PC, uncoordinated PC, and lithium ion, respectively, N is the average solvation number, and $A_{PC\,C}$ and $A_{PC\,UC}$ are relative areas of the IR bands for coordinated PC and uncoordinated PC, respectively.

$$C_{PC\,C} = NC_{Li}$$

$$C_{PC\,C} = \frac{A_{PC\,C}}{A_{PC\,C} + A_{PC\,UC}} C_{PC}$$

$$N = \frac{A_{PC\,C}}{A_{PC\,C} + A_{PC\,UC}} \frac{C_{PC}}{C_{Li}} \quad (2)$$

The number of PC molecules coordinated to the lithium cation (solvation number) decreases with increasing concentration of $LiPF_6$ (Figure 4). The decrease in solvation number coincides with the increase in the intensity of the $LiPF_6$ absorptions at 877 and 834 cm^{-1} characteristic of ion pairs.[37] The changes in the IR spectral properties are consistent with a change in solution structure. The predominant structure in solution, at low concentrations of $LiPF_6$ (1.2 M), is a tetra-PC solvated lithium cation with a solvent-separated PF_6^- anion. At high concentrations of $LiPF_6$ (3.0 M), the predominant structure in solution is a tri-PC coordinated cation-contact ion pair (Scheme 1).[37] The change in solution structure correlates with a change in the reversibility of the cycling of lithium ion cells.

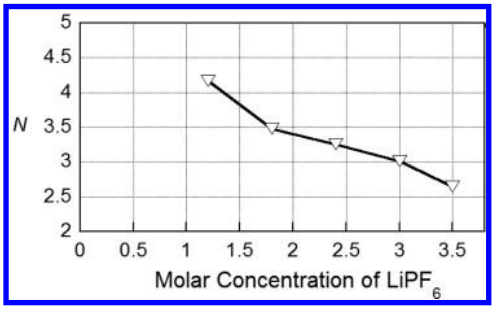

Figure 4. Number of PC molecules (N) coordinated to the Li cation at different $LiPF_6$ concentrations.

DOSY NMR Analysis of Multinuclear Diffusion in $LiPF_6$/PC Electrolytes. In an effort to better understand the solution structure of $LiPF_6$/PC electrolytes and the interactions between the Li^+ cation and the PF_6^- anion, diffusion rates were monitored as a function of [$LiPF_6$]. The diffusion coefficients

dx.doi.org/10.1021/jp409765w | J. Phys. Chem. C 2013, 117, 25381−25389

Scheme 1

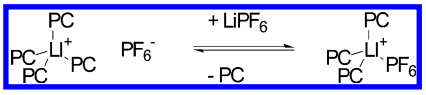

(D) of Li^+ and PF^-_6 in electrolytes have been determined by ^7Li and ^{19}F DOSY NMR, via linear fitting of plots of ln(I) versus G_i^2. A representative data set is provided in the Supporting Information (Figure SI4). The diffusion coefficients of Li^+ and PF_6^- at three different concentrations of $LiPF_6$ in PC are provided in Table 1. Both Li^+ and PF_6^- diffuse at slower rates at higher salt concentrations, which is not surprising due to the increased viscosity of electrolytes with high salt content.[38]

Table 1. Diffusion Coefficients As Determined by ^7Li and ^{19}F DOSY NMR Spectroscopy at 298 K for Three Concentrations of Electrolyte

^7Li DOSY	D, m^2/s
1.2 M $LiPF_6$/PC	6.68×10^{-11}
2.4 M $LiPF_6$/PC	1.23×10^{-11}
3.5 M $LiPF_6$/PC	5.12×10^{-12}
^{19}F DOSY	D, m^2/s
1.2 M $LiPF_6$/PC	1.20×10^{-10}
2.4 M $LiPF_6$/PC	1.95×10^{-11}
3.5 M $LiPF_6$/PC	7.69×10^{-12}

However, it is more informative to compare the diffusion coefficients of Li^+ and PF_6^- at the same concentration of salt. For 1.2 M $LiPF_6$ in PC, the diffusion coefficient of Li^+ cation is 6.68^{-11} m^2/s, which is about one-half of the ^{19}F diffusion coefficient 1.20^{-10} m^2/s of the PF_6^- anion, suggesting that transport of the Li^+ cation is slower than the transport of PF_6^- anion. This is consistent with lithium ion solvation in the presence of weakly coordinating anions because the Li^+ cation is typically strongly coordinated by four solvent molecules (PC), while the PF_6^- has weaker interactions with the solvent molecules. Thus, the larger coordinated Li^+ cation diffuses slower than the smaller uncoordinated PF_6^- anion. The difference of the diffusion coefficients for the Li^+ cation and the PF_6^- anion becomes smaller as the concentration of $LiPF_6$ is increased. Upon increasing the concentration of $LiPF_6$ to 2.4 M in PC, the diffusion constants of the Li^+ cation and the PF_6^- anion are 1.23^{-11} and 1.95^{-11} m^2/s, respectively, while on further increasing the concentration of $LiPF_6$ to 3.5 M in PC, the diffusion constants of the Li^+ cation and the PF_6^- anion are 5.12^{-12} and 7.69^{-12} m^2/s. The ratio of the diffusion constant of Li^+ cation to the PF_6^- anion changes from 1:1.8 to 1:1.5 upon increasing the $LiPF_6$ concentration from 1.2 to 3.5 M. The changes in diffusion rates are consistent with a change in solution structure from solvent-separated ion pairs to contact ion pairs upon increasing the concentration of $LiPF_6$.

TEM and EDX Analysis of BF Graphite Electrodes. Binder-free graphite electrodes were prepared with integrated copper TEM grids allowing straightforward TEM analysis without additional treatment.[36] The cells were cycled with five concentrations of $LiPF_6$ in PC (1.2, 2.4, 2.8, 3.0, and 3.5 M) dismantled, and TEM images were acquired (Figure 5). The graphite particles cycled with different concentrations of $LiPF_6$ have significantly different surface films. Graphite particles cycled in the presence of 1.2 M $LiPF_6$ in PC are very similar to the fresh graphite particles. There is no significant change in the appearance of the surface. EDX analysis reveals the elemental composition at two points of the graphite particle, the edge and

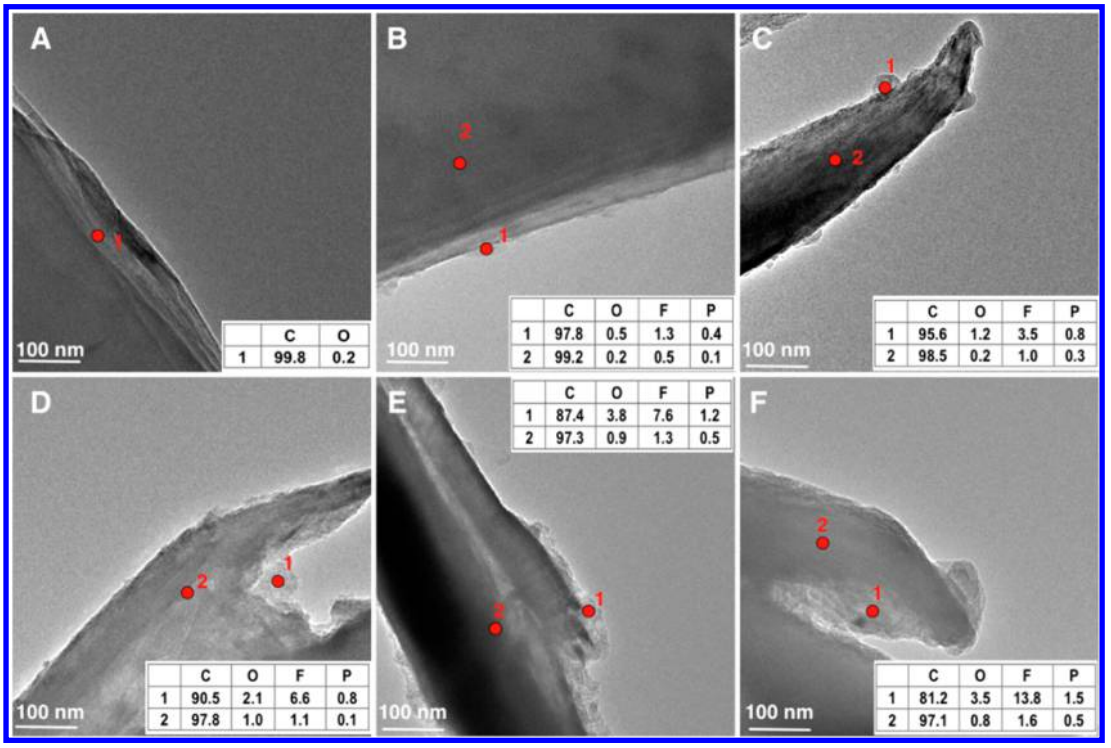

Figure 5. TEM bright-field images of fresh graphite and graphite anodes cycled with five concentrations of $LiPF_6$/PC electrolytes. (A) Fresh graphite electrode, (B) 1.2 M, (C) 2.4 M, (D) 2.8 M, (E) 3.0 M, and (F) 3.5 M. The inset indicates the element composition detected by EDX. The red spots indicate locations probed by EDX.

dx.doi.org/10.1021/jp409765w | J. Phys. Chem. C 2013, 117, 25381−25389

the center (inset of Figure 5B). A slight increase in the concentration of O, F, and P is observed on the edge of the graphite particle as compared to the bulk graphite consistent with the presence of low concentrations of electrolyte decomposition products. This is surprising because cells cycled with 1.2 M $LiPF_6$ in PC observe continuous electrolyte reduction at 0.9 V, which would be expected to generate a high concentration of electrolyte reduction products. However, it appears that the electrolyte reduction products of 1.2 M $LiPF_6$ in PC either do not adhere strongly to the surface of the graphite particles or are readily dissolved during the DMC rinsing of the electrodes.[29,39] In either case, the electrolyte decomposition products do not passivate the surface of the graphite electrode resulting in consistent electrolyte reduction.

As the concentration of $LiPF_6$ is increased, the presence of electrolyte decomposition products on the surface of the graphite particles becomes more apparent. Upon increasing the concentration to 2.4 M, a thin and uniform film is observed on the edge of the graphite particles. The thickness of the film is approximately 5 nm and has an increased concentration of F and O, 3.5% and 1.2%, respectively. A further increase in the concentration of $LiPF_6$ to 2.8 M results in the generation of a thicker surface film on the graphite particle. In addition, the concentrations of F and O are increased to 6.6% and 2.1%, respectively. The presence of higher concentrations of F and O on the graphite surface coincides with the onset of reversible cycling, as described above, and is characteristic of the formation of a passivating SEI.[36] At 3.5 M, a grainy thin film (~50 nm) is observed coating the entire graphite particle, and the concentrations of F and O at the surface are further increased to 13.8 and 3.5, respectively. Interestingly, the ratio of F to O is relatively constant at ~3:1 for all of the surface films, which suggests that the F content is much higher than for the SEI generated for 1.2 M $LiPF_6$ in EC that contained an SEI with a 1:1 ratio of F to O.[36]

NMR Spectroscopy of D_2O Extracts of BF-Graphite Electrodes. In an effort to characterize the components of the SEI on BF-graphite electrodes cycled with $LiPF_6$ in PC, the cycled electrodes were extracted from the cells, rinsed with DMC to remove residual electrolyte, and then extracted with D_2O to dissolve the SEI components. The D_2O extracts were analyzed by ^1H, ^{13}C, and ^{19}F NMR spectroscopy (Figure 6). The ^1H NMR spectra of the D_2O extract from a BF-graphite anode cycled with 1.2 M $LiPF_6$ in PC contain a single set of resonances at 1.10 ppm (d, 6.4 Hz), 3.35 ppm (dd, 11.6, 6.8 Hz), 3.45 ppm (dd, 11.6, 4.1 Hz), and 3.81 ppm (mult). The ^{13}C and DEPT-135 NMR spectra of the sample revealed four resonances at 17.96 ppm (methyl), 66.57 ppm (methylene), 67.91 ppm (methine), and 162.25 ppm (carbonyl) (Supporting Information Figure SI5). In addition, there is no evidence for the presence of significant concentrations of Li_2CO_3 (168.21 ppm) by ^{13}C NMR spectroscopy. The chemical shifts and the coupling constants are identical to the previously reported spectra for lithium propylene dicarbonate (LPDC), while COSY and HSQC NMR spectroscopy provide additional support of the structure (Supporting Information Figure SI5).[40] Thus, the predominant organic electrolyte decomposition product is LPDC. The ^{19}F NMR spectra reveal a doublet at −73.4 ppm and a singlet at −123 ppm characteristic of residual $LiPF_6$ and LiF. The ^1H, ^{13}C, and ^{19}F NMR spectra of the D_2O extract of the BF-graphite anode cycled with 3.5 M $LiPF_6$ are very similar, but the relative concentrations of the species are dramatically different. The ^1H NMR spectra reveal much lower

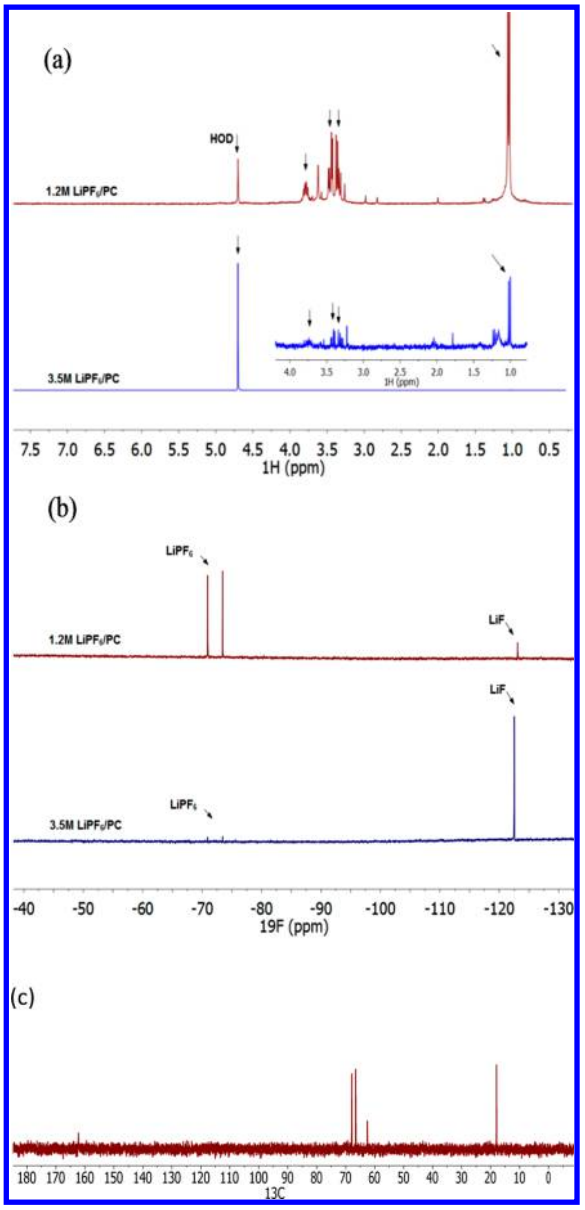

Figure 6. (a) ^1H NMR spectra, (b) ^{19}F NMR spectra of anodes extracted from 1.2 and 3.5 M $LiPF_6$/PC electrolytes, and (c) ^{13}C NMR spectrum of sample extracted from 1.2 M $LiPF_6$/PC electrolyte.

concentrations of LPDC, while the ^{19}F NMR spectra reveal much higher concentrations of LiF, as compared to the extract of the electrode cycled with 1.2 M $LiPF_6$ in PC. This suggests that at low concentrations of $LiPF_6$ the predominant reduction product of the electrolyte is LPDC, while at high concentrations of $LiPF_6$ the predominant reduction product is LiF. Further confirmation of the presence of LPDC was obtained via direct injection of the D_2O extract of the electrode cycled with 1.2 M $LiPF_6$ into a high-resolution electrospray ionization mass spectrometer (Supporting Information Table SI1 and Figures SI6,SI7). The absolute mass of the parent ion under positive ion mode is consistent with the presence of propylene dicarbonic acid (exact, 164.0321; found, 164.0329), confirming the presence of LPDC on the surface of the cycled anode.

The TEM images were also acquired on cycled graphite anode after D_2O extraction to remove the SEI to confirm quantitative removal. A TEM image of an anode cycled with 3.5 M electrolyte after D_2O extraction is depicted in Supporting

dx.doi.org/10.1021/jp409765w | J. Phys. Chem. C 2013, 117, 25381−25389

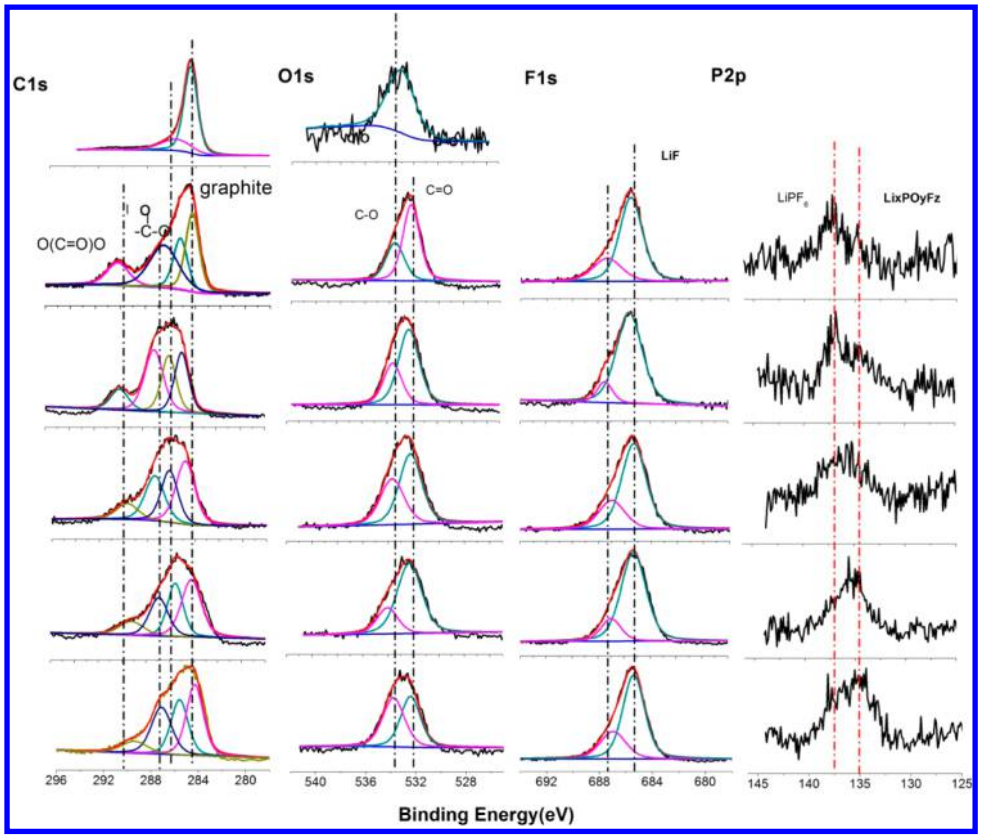

Figure 7. XPS spectra of fresh BF-graphite electrodes and BF-graphite electrodes extracted from coin cells cycled with $LiPF_6$/PC. From top: fresh BF-graphite electrode, 1.2, 2.4, 2.8, 3.0, and 3.5 M $LiPF_6$/PC electrolytes.

Information Figure SI8, and the elemental concentrations as determined by EDX are provided within the inset. The image and the elemental concentrations are very similar to those of uncycled graphite electrode, suggesting that the D_2O extraction removes all of the SEI components, which can be subsequently characterized by solution NMR spectroscopy.

Surface Analysis of Cycled BF-Graphite Electrodes by XPS. The surface of extracted BF-graphite electrodes was analyzed by XPS after cycling with 1.2, 2.4, 2.8, 3.0, and 3.5 M $LiPF_6$ in PC. The XPS spectra are presented in Figure 7, and the elemental concentrations are summarized in Table 2. The

Table 2. Element Percentage from BF-Anodes Cycled with Five Concentrations of $LiPF_6$/PC Electrolytes

	C%	O%	F%	P%
fresh	95.5	4.5		
1.2 M $LiPF_6$/PC	48.7	28.3	21.8	1.1
2.4 M $LiPF_6$/PC	47.1	27.6	23.7	1.3
2.8 M $LiPF_6$/PC	38.5	24.4	35.0	2.0
3.0 M $LiPF_6$/PC	37.5	19.5	40.8	2.1
3.5 M $LiPF_6$/PC	36.9	19.3	41.5	2.3

absence of binder in the BF-graphite electrodes allows a more accurate measurement of the surface element concentrations and avoids spectral overlap with binder. The C1s spectrum of the fresh BF-graphite electrode is dominated by the peak of graphite at 284.5 eV but also contains a low concentration of a peak at 286 eV consistent with surface oxidation of the graphite. A weak peak characteristic of C−O containing species is observed in the O1s spectrum at 533.8 eV characteristic of surface oxidation of the graphite.[41] Upon cycling with 1.2 M $LiPF_6$ in PC electrolyte, the XPS spectra change significantly. The concentrations of C are decreased, while the concentrations of O, F, and P are increased (Table 2). The C1s spectrum contains new peaks at ∼287 and 290 eV characteristic of C−O and C═O containing species. This is further supported by the O1s spectrum, which has a new strong peak at 532−533 eV, consistent with the presence of C−O (533 eV) and C═O (532 eV) containing species supporting the presence of LPDC, as observed by NMR spectroscopy described above.[42] In addition, a significant peak associated with graphite is observed at 284.5 eV consistent with the exposed graphite surface observed by TEM. This suggests that the reduction of PC is occurring at the BF-graphite electrode; however, the LPDC being generated is not adhering to the surface of the graphite particles and is instead being trapped in the pores of the electrode. The F1s spectrum contains a strong peak characteristic of LiF at 685 eV along with a weak shoulder at 687 eV characteristic of residual $LiPF_6$. The corresponding P2p peak for residual $LiPF_6$ is also observed at 138 eV.

Upon steadily increasing the concentration of $LiPF_6$ from 1.2 to 3.5 M, the concentrations of C and O systematically decrease, while the concentrations of F and P increase. The C1s spectra of electrodes cycled with 2.4−3.5 M $LiPF_6$ in PC remain dominated by the C═O, C−O, and graphite peaks at 290, 287, and 284.5 eV, respectively. Likewise, the O1s spectra of electrodes cycled with 2.4−3.5 M $LiPF_6$ are dominated by the C−O and C═O peaks at 533 and 532 eV, respectively. This is consistent with the C- and O-containing species being predominantly LPDC and graphite, which is in agreement with the NMR and TEM data. In addition, the decrease in concentration of C and O on the surface of the electrodes

dx.doi.org/10.1021/jp409765w | J. Phys. Chem. C 2013, 117, 25381−25389

correlates with ^{1}H NMR spectra of the D_2O extracts, which indicate that the concentration of LPDC decreases upon increasing the concentration of $LiPF_6$. While the presence of C−O and C═O species could also support the presence of Li_2CO_3 on the surface of the BF graphite electrodes, there is not clear support for the presence of significant concentrations of Li_2CO_3 by ^{13}C NMR, as discussed above. The F1s spectra of electrodes cycled with 2.4−3.5 M $LiPF_6$ contain a strong peak at 685 eV characteristic of LiF and a shoulder at 687 eV characteristic of $LiPF_6$ or $Li_xPF_yO_z$. Weak peaks are also observed in the P2p spectra consistent with low concentrations of $Li_xPO_yF_z$ (135 eV) and residual $LiPF_6$ (138 eV). The increase in concentration of F from 21.8% to 41.5% as observed by XPS upon increasing the concentration of $LiPF_6$ in PC from 1.2 to 3.5 M is consistent with the increased concentrations of LiF observed by NMR spectroscopy. The large increase of fluorine in the SEI is consistent with more decomposition of $LiPF_6$ for cells cycled with electrolytes containing higher concentrations of $LiPF_6$. Thus, the XPS data are consistent with the results observed by TEM-EDX and NMR, suggesting that SEI on the BF-graphite electrodes is primarily composed of LPDC and LiF. However, when the cells cycle reversibly, at high concentrations of $LiPF_6$, the SEI is dominated by LiF with low concentrations of LPDC. When the cells do not cycle reversibly and experience continuous electrolyte reduction, at low concentrations of $LiPF_6$, the dominate reduction product is LPDC with a low concentration of LiF, which does not passivate the graphite surface.

SUMMARY AND CONCLUSIONS

The cycling performance of $LiPF_6$/PC electrolytes with graphite electrodes changes as a function of the $LiPF_6$ concentration. At low $LiPF_6$ concentrations, continuous electrolyte reduction is observed at ∼0.9 V vs Li, and lithiation of the graphitic anode does not occur. At high concentrations of $LiPF_6$, a shoulder is observed at 0.8 V vs Li consistent with SEI formation, and a plateau is observed from 0.3 to 0.05 V vs Li consistent with reversible lithiation/delithiation of graphite. Cyclic voltammetry provides analogous results supporting reversible lithiation/delithiation only at high concentrations of $LiPF_6$. IR spectroscopy of $LiPF_6$/PC electrolytes reveals the presence of both PC coordinated to the Li^+ and uncoordinated PC. Modeling of the C═O stretching region provides an estimate of the number of PC molecules coordinated to each Li^+. As the concentration of $LiPF_6$ is gradually increased from 1.2 to 3.0 M, the PC solvation number gradually decreases from 4 to 3. In addition, at high concentrations of $LiPF_6$, the absorptions characteristic of PF_6^- are consistent with the presence of a contact ion pair. A shift from solvent-separated ion pair at low $LiPF_6$ concentration to a contact ion pair at high $LiPF_6$ concentration is also supported by DOSY NMR spectroscopy. Thus, the change in cycling behavior clearly correlates with the change in solution structure.

To better understand why the change in solution structure alters the cycling performance, ex situ surface analysis of the cycled electrodes has been conducted. At low concentrations of $LiPF_6$, the individual graphite particles contain a very thin surface film (∼5 nm) as determined by TEM with EDX. However, the bulk electrode contains a high concentration of lithium propylene dicarbonate (LPDC) as determined by a combination of XPS and solution NMR spectroscopy of the D_2O extracts of the electrode. Continuous electrolyte reduction generates LPDC as the dominant product, but the LPDC does not adhere well to the graphite surface and thus does not passivate the surface and subsequently inhibit further electrolyte reduction. At high concentrations of $LiPF_6$, the surface analysis provides very different results. The individual graphite particles contain a thick surface film (∼50 nm) with a high concentration of F as determined by TEM with EDX. The SEI contains a high concentration of LiF and a low concentration of LPDC as determined by XPS and solution NMR spectroscopy of the D_2O extracts of the electrode. Thus, at high concentrations of $LiPF_6$, the predominant reduction product of the electrolyte is LiF, which adheres well to the surface of the graphite particles, forming a stable SEI that inhibits further electrolyte reduction.

The results are summarized in Scheme 2. At low concentrations of $LiPF_6$, the predominant solution structure

Scheme 2

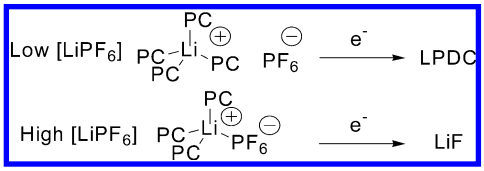

is the solvent-separated ion pair. Upon charging the cell, the principal reduction product of the solvent-separated ion pair is LPDC, which does not passivate the electrode surface, and the electrolyte is continuously reduced. At high concentrations of $LiPF_6$, the predominant structure is the contact ion pair. Upon charging the cell, the principal reduction product of the contact ion pair is LiF, with a low concentration of LPDC to enhance the Li ion conduction, which passivates the electrode surface, allowing efficient lithiation/delithiation of the graphite electrode.

ASSOCIATED CONTENT

Supporting Information

Additional figures and tables. This material is available free of charge via the Internet at http://pubs.acs.org.

AUTHOR INFORMATION

Corresponding Author

*E-mail: blucht@chm.uri.edu.

Notes

The authors declare no competing financial interest.

ACKNOWLEDGMENTS

We gratefully acknowledge funding from the Department of Energy Office of Basic Energy Sciences EPSCoR Implementation award (DE-SC0007074).

REFERENCES

(1) Goodenough, J. B. Evolution of Strategies for Modern Rechargeable Batteries. *Acc. Chem. Res.* **2013**, *46*, 1053−1061.

(2) Xu, K. Nonaqueous Liquid Electrolytes for Lithium-Based Rechargeable Batteries. *Chem. Rev.* **2004**, *104*, 4304−4417.

(3) Verma, P.; Maire, P.; Novák, P. A Review of the Features and Analyses of the Solid Electrolyte Interphase in Li-Ion Batteries. *Electrochim. Acta* **2010**, *55*, 6332−6341.

(4) Peled, E. The Electrochemical Behavior of Alkali and Alkaline Earth Metals in Nonaqueous Battery Systems−The Solid Electrolyte Interphase Model. *J. Electrochem. Soc.* **1979**, *126*, 2047−2051.

(5) Aurbach, D. Review of Selected Electrode−Solution Interactions which Determine the Performance of Li and Li Ion Batteries. *J. Power Sources* **2000**, *89*, 206−218.
(6) Xu, K.; von Cresce, A. Interfacing Electrolytes with Electrodes in Li Ion Batteries. *J. Mater. Chem.* **2011**, *21*, 9849−9864.
(7) Niehoff, P.; Passerini, S.; Winter, M. Interface Investigations of a Commercial Lithium Ion Battery Graphite Anode Material by Sputter Depth Profile X-ray Photoelectron Spectroscopy. *Langmuir* **2013**, *29*, 5806−5816.
(8) Besenhard, J. O.; Winter, M.; Yang, J.; Biberacher, B. Filming Mechanism of Lithium-Carbon Anodes in Organic and Inorganic Electrolytes. *J. Power Sources* **1995**, *54*, 228−231.
(9) Schechter, A.; Aurbach, D.; Cohen, H. *Langmuir* **1999**, *15*, 3334−3342.
(10) Winter, M. The Solid Electrolyte Interphase − The Most Important and the Least Understood Solid Electrolyte in Rechargeable Li Batteries. *Z. Phys. Chem.* **2009**, *223*, 1395−1406.
(11) von Cresce, A.; Xu, K. Preferential Solvation of Li^+ Directs Formation of Interphase on Graphitic Anode. *Electrochem. Solid-State Lett.* **2011**, *14*, A154−A156.
(12) Yamada, Y.; Koyama, Y.; Abe, T.; Ogumi, Z. Correlation between Charge−Discharge Behavior of Graphite and Solvation Structure of the Lithium Ion in Propylene Carbonate-Containing Electrolytes. *J. Phys. Chem. C* **2009**, *113*, 8948−8953.
(13) Barthel, J.; Deser, R. FTIR Study of Ion Solvation and Ion-Pair Formation in Alkaline and Alkaline Earth Metal Salt Solutions in Acetonitrile. *J. Solution Chem.* **1994**, *23*, 1133−1146.
(14) Cazzanelli, E.; Croce, F.; Appetecchi, G. B.; Benevelli, F.; Mustarelli, P. Li[Sup +] Solvation in Ethylene Carbonate–Propylene Carbonate Concentrated Solutions: A Comprehensive Model. *J. Chem. Phys.* **1997**, *107*, 5740−5747.
(15) Barthel, J.; Buchner, R.; Wismeth, E. FTIR Spectroscopy of Ion Solvation of LiClO4 and LiSCN in Acetonitrile, Benzonitrile, and Propylene Carbonate. *J. Solution Chem.* **2000**, *29*, 937−954.
(16) Alía, J. M.; Edwards, H. G. M. Ion Solvation and Ion Association in Lithium Trifluoromethanesulfonate Solutions in Three Aprotic Solvents. An Ft-Raman Spectroscopic Study. *Vib. Spectrosc.* **2000**, *24*, 185−200.
(17) Tasaki, K.; Goldberg, A.; Liang, J.; Winter, M. New Insight into Differences in Cycling Behaviors of a Lithium-ion Battery Cell Between the Ethylene Carbonate- and Propylene Carbonate-Based Electrolytes. *J. Electrochem. Soc.* **2011**, *33*, 59−69.
(18) von Wald Cresce, A.; Borodin, O.; Xu, K. Correlating Li+ Solvation Sheath Structure with Interphasial Chemistry on Graphite. *J. Phys. Chem. C* **2012**, *116*, 26111−26117.
(19) Yang, L.; Xiao, A.; Lucht, B. L. Investigation of Solvation in Lithium Ion Battery Electrolytes by NMR Spectroscopy. *J. Mol. Liq.* **2010**, *154*, 131−133.
(20) Seo, D. M.; Borodin, O.; Han, S.-D.; Ly, Q.; Boyle, P. D.; Henderson, W. A. Electrolyte Solvation and Ionic Association I. Acetonitrile-Lithium Salt Mixtures: Intermediate and Highly Associated Salts. *J. Electrochem. Soc.* **2012**, *159*, A553−A565.
(21) Fong, R.; von Sacken, U.; Dahn, J. R. Studies of Lithium Intercalation into Carbons Using Nonaqueous Electrochemical Cells. *J. Electrochem. Soc.* **1990**, *137*, 2009−2013.
(22) Herstedt, M.; Andersson, A. M.; Rensmo, H.; Siegbahn, H.; Edström, K. Characterisation of the SEI Formed on Natural Graphite in PC-Based Electrolytes. *Electrochim. Acta* **2004**, *49*, 4939−4947.
(23) Inaba, M.; Siroma, Z.; Kawatate, Y.; Funabiki, A.; Ogumi, Z. Electrochemical Scanning Tunneling Microscopy Analysis of the Surface Reactions on Graphite Basal Plane in Ethylene Carbonate-Based Solvents and Propylene Carbonate. *J. Power Sources* **1997**, *68*, 221−226.
(24) Jeong, S.-K.; Inaba, M.; Iriyama, Y.; Abe, T.; Ogumi, Z. AFM Study of Surface Film Formation on a Composite Graphite Electrode in Lithium-Ion Batteries. *J. Power Sources* **2003**, *119−121*, 555−560.
(25) Chung, G. C.; Kim, H. J.; Yu, S. I.; Jun, S. H.; Choi, J. w.; Kim, M. H. Origin of Graphite Exfoliation an Investigation of the Important Role of Solvent Cointercalation. *J. Electrochem. Soc.* **2000**, *147*, 4391−4398.
(26) Wang, J.; Manga, K. K.; Bao, Q.; Loh, K. P. High-Yield Synthesis of Few-Layer Graphene Flakes through Electrochemical Expansion of Graphite in Propylene Carbonate Electrolyte. *J. Am. Chem. Soc.* **2011**, *133*, 8888−8891.
(27) Tasaki, K. Solvent Decompositions and Physical Properties of Decomposition Compounds in Li-Ion Battery Electrolytes Studied by DFT Calculations and Molecular Dynamics Simulations. *J. Phys. Chem. B* **2005**, *109*, 2920−2933.
(28) Aurbach, D.; Daroux, M. L.; Faguy, P. W.; Yeager, E. Identification of Surface Films Formed on Lithium in Propylene Carbonate Solutions. *J. Electrochem. Soc.* **1987**, *134*, 1611−1620.
(29) Xu, K. Whether EC and PC Differ in Interphasial Chemistry on Graphitic Anode and How. *J. Electrochem. Soc.* **2009**, *156*, A751−A755.
(30) Abe, K.; Yoshitake, H.; Kitakura, T.; Hattori, T.; Wang, H.; Yoshio, M. Additives-Containing Functional Electrolytes for Suppressing Electrolyte Decomposition in Lithium-Ion Batteries. *Electrochim. Acta* **2004**, *49*, 4613−4622.
(31) Aurbach, D.; Gamolsky, K.; Markovsky, B.; Gofer, Y.; Schmidt, M.; Heider, U. On the Use of Vinylene Carbonate (VC) Electrolyte Solutions for Li-Ion as an Additive to Batteries. *Electrochim. Acta* **2002**, *47*, 1423−1439.
(32) Zhuang, G. V.; Xu, K.; Jow, T. R.; Ross, P. N., Jr. Study of SEI Layer Formed on Graphite Anodes in PC/LiBOB Electrolyte Using IR Spectroscopy. *Electrochem. Solid-State Lett.* **2004**, *7*, A224−A227.
(33) Jeong, S.-K.; Inaba, M.; Iriyama, Y.; Abe, T.; Ogumi, Z. J. Interfacial Reactions Between Graphite Electrodes and Propylene Carbonate-Based Solutions: Electrolyte-Concentration Dependence of Electrochemical Lithium Intercalation Reaction. *J. Power Sources* **2008**, *175*, 540−546.
(34) Kang, S. H.; Abraham, D. P.; Xiao, A.; Lucht, B. L. Investigating the Solid Electrolyte Interphase Using Binder-Free Graphite Electrodes. *J. Power Sources* **2008**, *175*, 526−532.
(35) Xiao, A.; Yang, L.; Lucht, B. L.; Kang, S.-H.; Abraham, D. P. Examining the Solid Electrolyte Interphase on Binder-Free Graphite Electrodes. *J. Electrochem. Soc.* **2009**, *156*, A318−A327.
(36) Nie, M.; Chalasani, D.; Abraham, D. P.; Chen, Y.; Bose, A.; Lucht, B. L. Lithium Ion Battery Graphite Solid Electrolyte Interphase Revealed by Microscopy and Spectroscopy. *J. Phys. Chem. C* **2013**, *117*, 1257−1267.
(37) Aroca, R.; Nazri, M.; Nazri, G. A.; Camargo, A. J.; Trsic, M. Vibrational Spectra and Ion-Pair Properties of Lithium Hexafluorophosphate in Ethylene Carbonate Based Mixed-Solvent Systems for Lithium Batteries. *J. Solution Chem.* **2000**, *29*, 1047−1060.
(38) Lencka, M. M.; Anderko, A.; Sanders, S. J.; Young, R. D. Modeling Viscosity of Multicomponent Electrolyte Solutions. *Int. J. Thermophys.* **1998**, *19*, 367−378.
(39) Ein-Eli, Y. A New Perspective on the Formation and Structure of the Solid Electrolyte Interface at the Graphite Anode of Li-Ion Cells. *Electrochem. Solid-State Lett.* **1999**, *2*, 212−214.
(40) Xu, K.; Zhuang, G. R. V.; Allen, J. L.; Lee, U.; Zhang, S. S.; Ross, P. N.; Jow, T. R. Syntheses and Characterization of Lithium Alkyl Mono- and Dicarbonates as Components of Surface Films in Li-Lon Batteries. *J. Phys. Chem. B* **2006**, *110*, 7708−7719.
(41) Andersson, A.; Abraham, D.; Haasch, R.; MacLaren, S.; Liu, J.; Amine, K. Surface Characterization of Electrodes from High Power Lithium-Ion Batteries. *J. Electrochem. Soc.* **2002**, *149*, A1358−A1369.
(42) Dedryvere, R.; Gireaud, L.; Grugeon, S.; Laruelle, S.; Tarascon, J. M.; Gonbeau, D. Characterization of Lithium Alkyl Carbonates by X-Ray Photoelectron Spectroscopy: Experimental and Theoretical Study. *J. Phys. Chem. B* **2005**, *109*, 15868−15875.